On Analysis Driven Shape Design Using B-Splines

Marlena C. Gomez*, Marshall C. Galbraith†, Robert Haimes ‡

Massachusetts Institute of Technology, Cambridge, MA, 02139

This paper presents a method for aerodynamic design using B-splines which aims to combine traditional CAD-like parametric solid model construction with freeform-like local deformation, all driven by optimization. Integrating the B-spline geometry with ESP's constructive solid modeling will allow the reshaping of parts of the full 3D geometric model and the creation of shape designs that can be considered "generative". The method uses B-splines and Engineering SketchPad (ESP) to construct the geometry, making the control point locations of certain B-splines available as the design parameters during optimization. This approach is demonstrated in morphing 2D airfoil and 3D wingtip shapes with CFD analysis using `Cart3D`.

Nomenclature

C_D	=	two-dimensional drag coefficient
C_L	=	two-dimensional lift coefficient
C_p	=	two-dimensional pressure coefficient
P	=	local pressure
$Pinf$	=	free stream pressure
$C(t)$	=	B-Spline curve function
P_i	=	B-Spline control point i
$N_{i,p}(t)$	=	B-Spline basis functions
T	=	B-Spline knot value vector
ϵ	=	integrated L^2-norm difference
s_i	=	L^2-norm error between two knots
ε_j	=	square error between two points on two splines at the same knot value
t_j	=	fractional distance between two knot values
w_j	=	weight of a coordinate c_j using Gaussian quadrature
U	=	knot vector in the u-direction
V	=	knot vector in the v-direction
$S(u,v)$	=	B-Spline surface function
M	=	Mach number
$\mathcal{J}$	=	objective function
$\mathcal{T}$	=	geometry triangulation
α	=	angle-of-attack

I. Introduction

Aerodynamic shape optimization has been the subject of extensive research. High-fidelity optimization techniques and tools have broadened from solving optimal configurations of simple airfoil geometries to more complex components [1–4]. Despite this progress, these tools have not been widely adopted among designers. While the compute resources required has improved with the use of the adjoint method to compute objective gradients [5], among the challenges still remaining in adopting high-fidelity aerodynamic shape optimization tools is the required depth of knowledge among a myriad of tool-sets.

Some of the many steps in using Computational Fluid Dynamics (CFD) to solve a shape optimization problem include geometry parameterization, surface and volume meshing, flow analysis, and the optimization itself. Consequently,

---

*Undergraduate Student, Computer Science and Engineering.

†Research Engineer, Department of Aeronautics & Astronautics, AIAA Senior member.

‡Principal Research Engineer, Department of Aeronautics & Astronautics, AIAA member.

in many cases an extensive knowledge of the design problem and setup is required. This is especially true in the case of optimization problems with larger sets of design variables, where automatic execution relies on specific setup requirements and careful orchestration. Ultimately, this results in the design process becoming less practical to design engineers [6]. Automation of this process offers a way to ease some restrictions and allows for decreased manual setup times. However, while various frameworks have integrated aspects of the shape optimization process, it is challenging to integrate all of the disparate codes involved in each step.

Historically, much of the reason for the wide array of codes involved in shape optimization stems from the geometric modelers used (if any). Among the aerospace design community, custom in-house discrete (mesh-based) tools are common. Furthermore, commercially available shape control systems that come in CAD-based and CAD-free forms both come with drawbacks [7]. Due to their proprietary nature, commercial CAD systems may hide core geometric components from the user/programmer, making it difficult to compute values like parametric sensitivities [8]. Furthermore, customization in commercial CAD systems can be difficult, which can make the time-consuming process of re-parameterization of the design before or during optimization necessary [9]. Additionally, the number of available CAD licenses can become a practical issue [10]. On the other hand, CAD-free systems can have limited intuitive shape design parameters (i.e., the design parameters of the system are purely mathematical and do not reflect the manner that designers understand the design space). These typically require time-consuming manipulation for custom shape design parameterization. For these reasons, methods of freeform parameterization for modeling geometry can help streamline the optimization process at the detriment of design engineers fully understanding the results.

B-splines can be used to bridge parametric solid modeling with freeform shape design. The result of constructive solid modeling can contain B-spline surfaces (and curves), and if not, the analytic geometry can be converted to B-splines. Highly flexible and efficient in approximation [11], B-splines are especially useful when there is not a clear means of parameterizing the geometry [12]. The proposed methodology builds on the idea of creating a general platform for local deformation and optimization of aerospace geometries using B-splines and the Engineering Geometry Aerospace Design System (EGADS) framework within Engineering SketchPad (ESP) [13]. Most aerodynamic shape optimization using CFD utilizes finite differencing to compute surface mesh sensitivities w.r.t. design variables within the adjoint approach when computing the objective function gradient for optimization [14]. However, in our methodology, operator overloaded automatic differentiation [15] is used which is more accurate and does not require geometric rebuilds for each parameter *in play*, making it far more efficient and robust.

Being able to adjust B-spline control point locations integrated with ESP's constructive solid modeling will allow for, at a later time in construction, the (re)shaping of parts of the geometric model. This form of mixed parametric builds (using traditional design parameters and B-spline control point locations) maintains the intuitive connection to the designer with parameters that are part of the discipline's lexicon with an additional suite of freeform parameters attached to various surfaces in the geometric model. If done properly, this combination of CAD-like and CAD-free parameterizations, when driven by the results of analysis (possibly in a multidisciplinary setting), can be considered "generative" design (a form finding process that can mimic nature's evolutionary approach). The mixed approach can be controlled in a way to avoid the pit-falls of Topological Optimization (used in structural design) where the optima are deep (and fragile in off-design) and the shapes need massaging before they can be manufactured. This paper discusses our mixed approach to shape optimization. The first section provides the fundamentals of B-splines. Then, the approach is demonstrated on an airfoil in 2D with and without CFD analysis. Following after are 3D airfoil design cases using B-Spline surfaces with CFD analysis. Cart3D design framework is used for the adjoint-based CFD analysis and shape optimization. The Cart3D design framework solves constrained aerodynamic shape optimization problems, using flow and adjoint solvers to compute the value of the objective function, constraints, and gradients at each design step [6].

II. 2D approach

A. B-splines

A B-spline, or basis spline, is a linear combination of a set of control points, $P_0, ...P_n$, and B-spline basis functions $N_{i,p}(t)$ given by:

$$C(t) = \sum_{i=0}^{n} P_i N_{i,p}(t) \tag{1}$$

where the basis functions:

$$N_{i,0}(t) = \begin{cases} 1 & \text{if } t_i \le t < t_{i+1} \\ 0 & \text{otherwise} \end{cases} \tag{2}$$

$$N_{i,j}(t) = \frac{t - t_i}{t_{i+j} - t_i} N_{i,j-1}(t) + \frac{t_{i+j+1} - t}{t_{i+j+1} - t_i + 1} N_{i+1,j-1}(t), \quad j \in [1, p] \tag{3}$$

are defined on a knot vector $T = \{t_0, t_1, ...t_m\}$ that is monotonically increasing with $t_i \in [0, 1]$. The knot values t_i are the places where the pieces of polynomial meet. The spline function has a degree of $p = m - n - 1$ [16]. In a normalized and non-periodic B-spline, the first and last knots are repeated $p + 1$ times. This multiplicity forces the endpoints of the curve to coincide with the first and last control points. For a knot vector with k duplicate knots, the B-Spline curve is $p - k$ differentiable. Thus the knot vector described by:

$$T = \{\underbrace{0, ..., 0}_{p+1}, t_{p+1}, ..., t_{m-p-1}, \underbrace{1, ..., 1}_{p+1}\} \tag{4}$$

creates a clamped B-spline curve, as seen in Fig. 1. Aside from the endpoints, each knot on the curve lies between two of the control points. In addition, aside form the endpoints, no control points lie on the B-Spline curve. The second to last control points at each end (P1 and P6 in Fig. 1) control the slope at the end of the spline. B-Spline knots and control points are often defined through a curve fitting process where the arc-length between a given series of points defines the knot sequence and the control points are positioned such that the spline passes through the fitting points. When doing a spline fit the points associated with the B-spline curve evaluated at the t-values coincides with the fitting points.
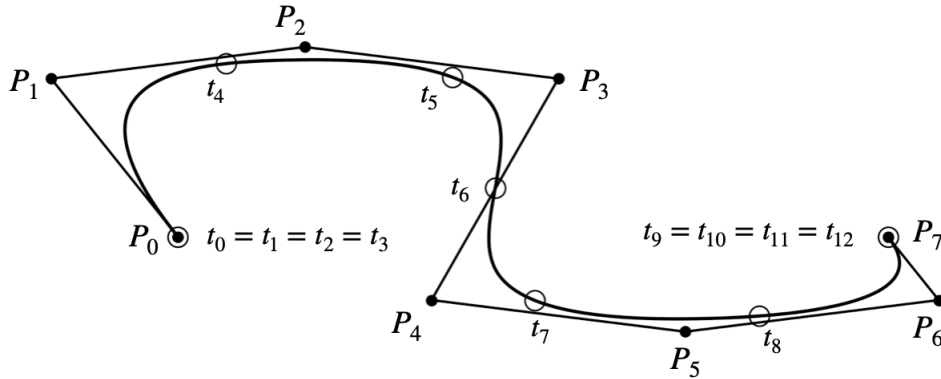
Fig. 1 **An example of a B-spline where P_i represents the control points of the spline and t_i represents the knots of the spline.**

B. Shape Design without Analysis

The shape design optimization process using B-Splines is first verified using gradient-based optimization for shape design without CFD analysis. The goal of this case is to validate the process by fitting B-splines to two NACA airfoils and morphing one airfoil B-spline to the other by minimizing the L^2-norm difference between the two splines. The knot sequence is identical between the two splines to simplify evaluating the $L^2 - norm$. The control points defining one of the spline fits are the free parameters in the optimization, with the exception of the first and last control points, which are fixed so the trailing edge does not open up.

First, two airfoil geometries are fit to cubic B-splines using a cosine distribution of parameter values for the NACA 4-series equations. The starting transient airfoil is fitted to the shape of a NACA 0012 airfoil and the target airfoil is fitted to the shape of a NACA 8416 airfoil, depicted in Fig. 2. The last coefficient of the NACA 4-series equations is changed from -0.1015 to -0.1036 to produce airfoils with a sharp trailing edge [17]. The B-spline curve defining each of the two airfoils is made up of 103 control points, and since all but the first and last control points can be modified, there are 101×2 (x-space and y-space) = 202 degrees of freedom. An `ego` structure is created for each airfoil using the EGADS framework in ESP [13] which stores the knots and control point information for the fitted B-Spline.

3

(a) NACA 0012   (b) NACA 8416

Fig. 2   The starting and target airfoil geometries.

The optimization minimizes the integrated L^2-norm difference between the starting NACA 0012 airfoil, which is transient, and the target NACA 8416 airfoil. The total L^2-norm error, ϵ, over a knot sequence of length m of the B-spline with degree p is computed as:

$$\epsilon = \sqrt{\sum_{i=p+1}^{m-p-1} s_i},$$ (5)

Every value s_i is the L^2-norm error calculated between two knot values:

$$s_i = \sum_{j=0}^{3} \varepsilon_j.$$ (6)

The value of ε_j is the square error of the two points (x_0, y_0) and (x_1, y_1) at the knot value t_j on the transient and target airfoils respectively, multiplied by the size of the interval:

$$\varepsilon_j = 2w_j(t_{i+1} - t_i)[(x_0 - x_1)^2 + (y_0 - y_1)^2], \quad j \in [0, 3]$$ (7)

The knot value t_j is the fractional distance between knots t_i and t_{i+1} computed by:

$$t_j = c_j(t_{i+1} - t_i) + t_i, \quad j \in [0, 3]$$ (8)

Each c_j is a coordinate computed by Gaussian quadrature. The Gaussian quadrature rule is defined as:

$$\int_0^1 f(x)dx \approx \sum_{i=1}^{n} w_i f(x_i).$$ (9)

Since both airfoils are fit to cubic B-Splines, the resulting polynomial from the square difference calculation has a degree of 6. A p-point Gaussian quadrature rule integrates an exact result for polynomials of degrees less than $2p - 1$, so a 4-point Gaussian quadrature, with values shown in Table 1, will integrate the L^2-norm exactly.

In order to use gradient-based optimization, the derivative of ϵ for every value of s_i is taken with respect to the control point i using operator overloaded automatic differentiation [15]. The derivatives are verified using finite differencing.

Table 1   4-point Gaussian Quadrature.

Index (j)	Coordinate (c_j)	Weight (w_j)
0	$\frac{1}{2}\sqrt{\frac{3}{7} - \frac{2}{7}\sqrt{\frac{6}{5}}}$	$\frac{1}{2}\frac{18+\sqrt{30}}{36}$
1	$-\frac{1}{2}\sqrt{\frac{3}{7} - \frac{2}{7}\sqrt{\frac{6}{5}}}$	$\frac{1}{2}\frac{18+\sqrt{30}}{36}$
2	$\frac{1}{2}\sqrt{\frac{3}{7} + \frac{2}{7}\sqrt{\frac{6}{5}}}$	$\frac{1}{2}\frac{18-\sqrt{30}}{36}$
3	$-\frac{1}{2}\sqrt{\frac{3}{7} + \frac{2}{7}\sqrt{\frac{6}{5}}}$	$\frac{1}{2}\frac{18-\sqrt{30}}{36}$

(a) Iteration 1

(b) Iteration 2

(c) Iteration 3

(d) Iteration 4
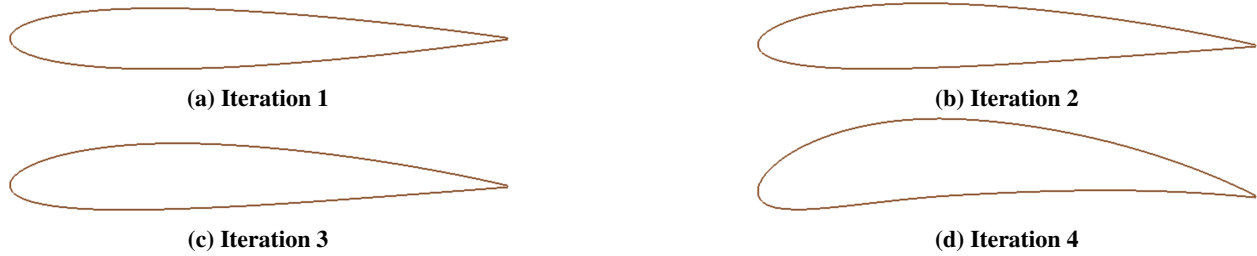
Fig. 3   The airfoil geometry resulting from the first 4 times the optimizer has evaluated the objective function. By the fourth evaluation the transient geometry appears to closely approximate a NACA 8416.

With Eq. 5 as the objective function, the optimization is performed using the NLopt [18] interface with the Low-store BFGS (Broyden–Fletcher–Goldfarb–Shanno) [19, 20] algorithm. The optimization terminates when the difference between the value of subsequent evaluations of the objective function is less than or equal to 1×10^{-17}. Within the first 5 evaluations, the NACA 0012 begins to approximate the NACA 4816 as shown in Fig. 3. Further evaluation continues to refine the geometry, with this gradient optimization stopping after 57 evaluations and the best result shown alongside the target spline fit in Fig. 4.

(a) The geometry resulting from optimization.

(b) The target NACA 8416.

Fig. 4   The resulting and target airfoils.

A derivative-free approach could be used for optimization, at a significant computational cost. In fact, for this example none of the derivative-free NLopt algorithms terminate within 100,000 objective function evaluations. The convergence history of the objective function value for the first 10,000 objective function evaluations of the NLopt derivative-free Constrained Optimization By Linear Approximations [21] algorithm is plotted along side the complete convergence history of the gradient-based algorithm in Fig. 5.
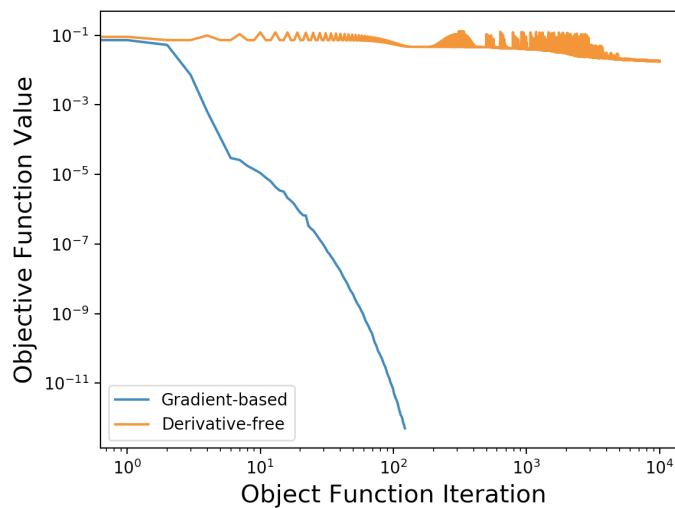
Fig. 5   Objective Function Convergence History

This result indicates that a gradient-based technique is necessary. Going from B-spline curves to surfaces will

only magnify this conclusion, since the surfaces will have many more control points, and, therefore, many more degrees-of-freedom in the optimization.

C. Shape Design with CFD Analysis

Figure 6 shows the workflow for shape design via CFD analysis using the `Cart3D` design framework [22]. The `Cart3D` design framework communicates between three applications via XML files. The XML files hold the geometric tessellation and tessellation sensitivities, the value of the optimization objective function, constraints, and their gradients, and, finally, the design variable values and bounds. The `Cart3D` design framework uses a "builder" application (which must be customized for the geometry of interest) to generate files with geometric tessellation files, the `Cart3D` solver uses the tessellation to compute the optimization objective and constraint values as well as their gradients, and finally an optimization application updates the design variables.

Here, an `EGADS` application, similar to `ESPxddm` [23], replaces the "builder" application. The `EGADS` app creates the geometry and tessellation based on design variable values from an XML input file using `EGADS` and outputs a `Cart3D` Trix file with the tessellation and tessellation sensitivities w.r.t. the design variables. The tessellation sensitivities are computed using the `EGADS` framework via the `EG_setGeometry_dot` and `EG_evalute_dot` functions. The sensitivity calculations computed with the `EGADS` application are verified with finite differencing.

`Cart3D` uses the tessellation to compute the objective function and constraint values as well as their gradients w.r.t. each design variable using an adjoint approach. These values and gradients are used by the optimizer to update the design variable values, which are transferred to the `EGADS` application via an XML file to generate the geometric tessellation for the next design iteration. The `Cart3D` design framework has two optimizers: gsearch and SNOPT [24]. The SNOPT algorithm is used for all the optimization cases in this paper.
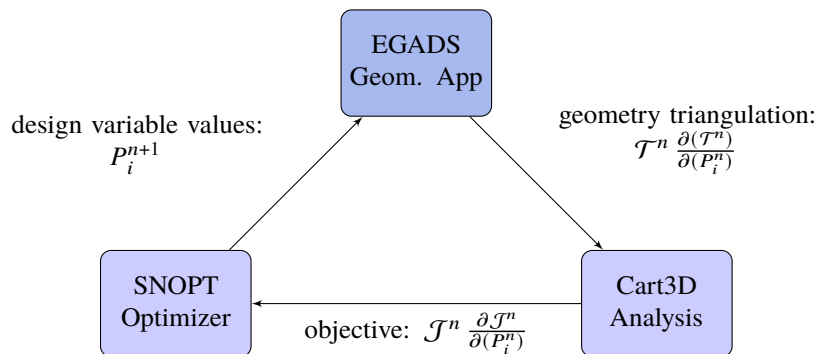
Fig. 6 Workflow of the shape design with CFD analysis optimization. P_i **represents a control point that is a design parameter for the optimization.**

Using this workflow, the results of case 1 in [25] are reproduced as another verification of using B-Spline control point locations for shape design with CFD analysis. This case minimizes drag of a symmetric, transonic, non-lifting airfoil. The starting airfoil is a modified NACA 0024 where the trailing edge is made sharp and fitted to a B-spline with 31 control points. The Mach number is 0.85 and the angle of attack is $\alpha = 0°$. The control points defining the upper half of the airfoil are the variables for the optimization. The control points on the lower surface are negated of the morphed upper surface control points to ensure the airfoil remains symmetric. The first and last control points (at $x = 0$ and $x = 1$) stay constant to prevent the tail and nose from opening up. The free control points are constrained to only move in the y-direction. The minimum y-constraint for each of these variables is the y-value of the corresponding control point in a B-spline fit of a NACA 0012 airfoil, as shown in Fig. 7.
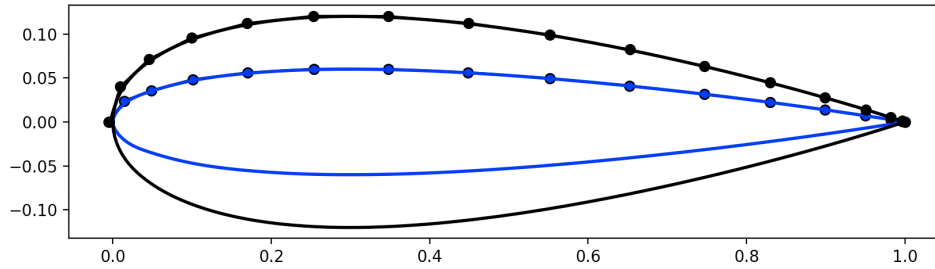
Fig. 7   The control points on the upper half of the NACA 0024 spline fit (in black), used as the design parameters with minimum y-constraints of the corresponding control point on the NACA 0012 spline fit (in blue).

The optimization uses a mesh of approximately 250,000 cells with 9 levels of adaptation. The resulting airfoil from the optimization is expected to be close to the results in Fig. 6 and Table 1 of [25], where the airfoil approaches a flat shape with a blunt nose to minimize drag. The results in Fig. 9 and Fig. 10 closely approximate the expected shape from the model case in the paper, though they are not identical. Figure 8 shows the convergence of the objective function over 17 design iterations, where drag is reduced from approximately 0.12 to 0.02. Figure 10 shows the pressure profiles of the initial airfoil and best shape found from the optimization. The optimized airfoil has significantly reduced the strength of the shock which leads to the reduction in drag.
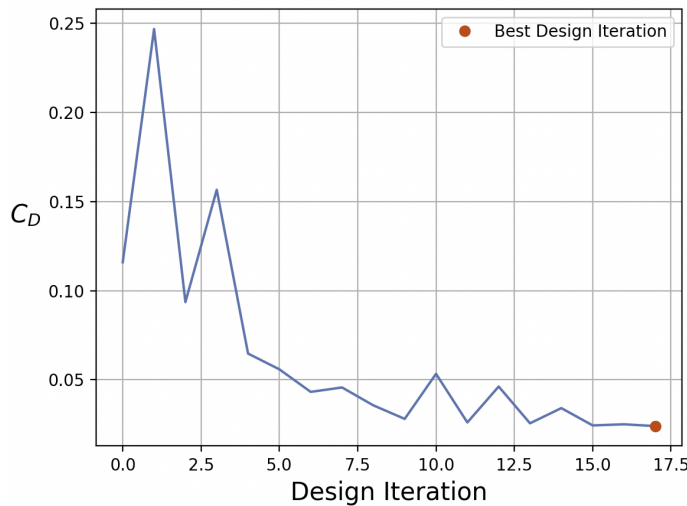
Fig. 8   Drag Convergence History.
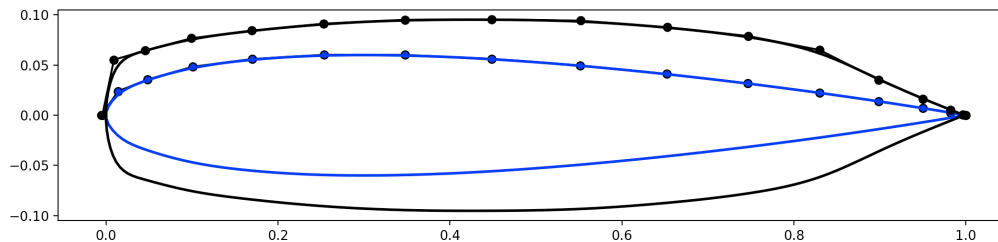
Fig. 9   The resulting spline defined by the control points in black, with the NACA 0012 minimum bounds in blue.

7
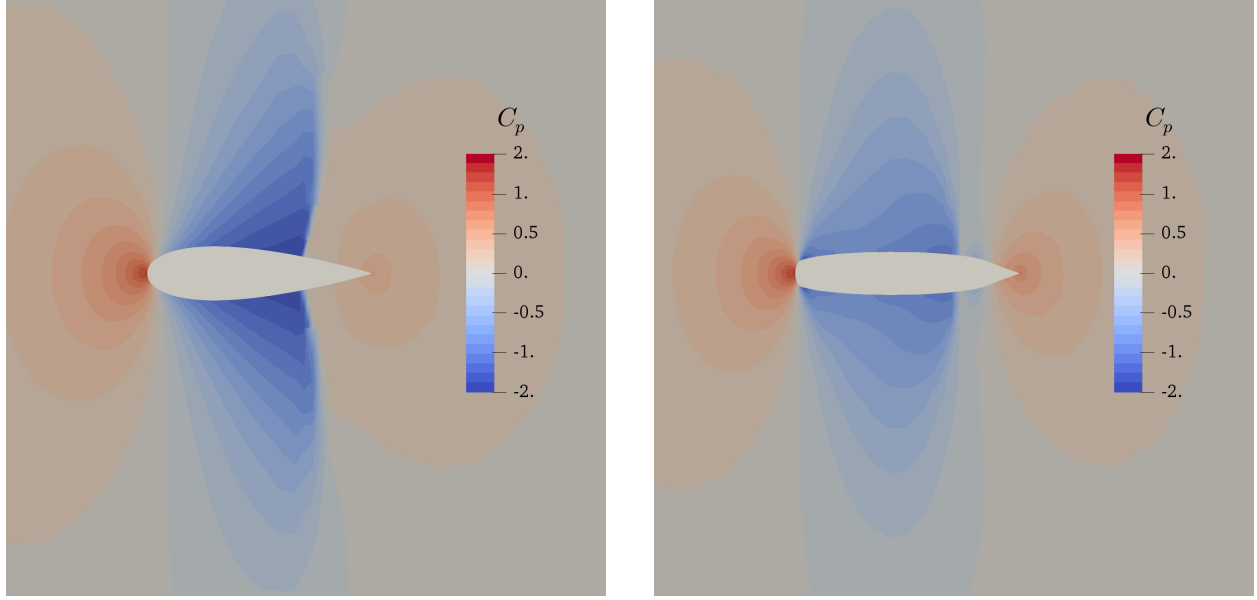
(a) The initial NACA 0024 airfoil.   **(b) The best airfoil found from optimization of drag.**

Fig. 10   The pressure profiles of the initial and best airfoils from the optimization.

III. 3D approach

Here, the method of using control point locations of B-Splines as design variables is extended from a 2D airfoil to a 3D wingtip. The wingtip is defined by a B-spline surface using the `EGADS` framework in ESP [26].

A. B-spline surfaces

A B-Spline surface, or patch, is defined by a topologically rectangular set of control points and two knot vectors in u and v directions. The surface is obtained as a tensor product of the bidirectional net of control points $P_{i,j}$ and the two knot vectors:

$$U = \{\underbrace{0, ..., 0}_{p+1}, u_{p+1}, ..., u_{r-p-1}, \underbrace{1, ..., 1}_{p+1}\}, \tag{10}$$

where U has $r + 1$ knots and $r = n + p + 1$, and

$$V = \{\underbrace{0, ..., 0}_{q+1}, u_{q+1}, ..., u_{rs-p-1}, \underbrace{1, ..., 1}_{q+1}\}, \tag{11}$$

where V has $s + 1$ knots and $s = m + q + 1$ [16]. The surface is then defined by:

$$S(u, v) = \sum_{i=0}^{n} \sum_{j=0}^{m} N_{i,p}(u) N_{j,q}(v) P_{i,j} \tag{12}$$

B. B-Spline Surface Optimization Set-Up

Using the `EGADS` framework in ESP, a B-Spline surface defining the wingtip of a NACA 0012 airfoil rectangular wing is made using the `blend` function with a radius of one. This method for creating the rounded wingtip is defined in more detail in the [27]. The number of control points to define the rounded wingtip was reduced from the default to 7 B-Spline rows lengthwise along the airfoil in order to reduce the number of design variables in the optimization. The airfoil has a unit chord, but the wingtip control points are not mirrored on the lower surface as they were in the 2D case. The surface and the complete net of control points are depicted in Fig. 11. There is a symmetry plane in the computational domain for the side of the wing that does not have a rounded wingtip.
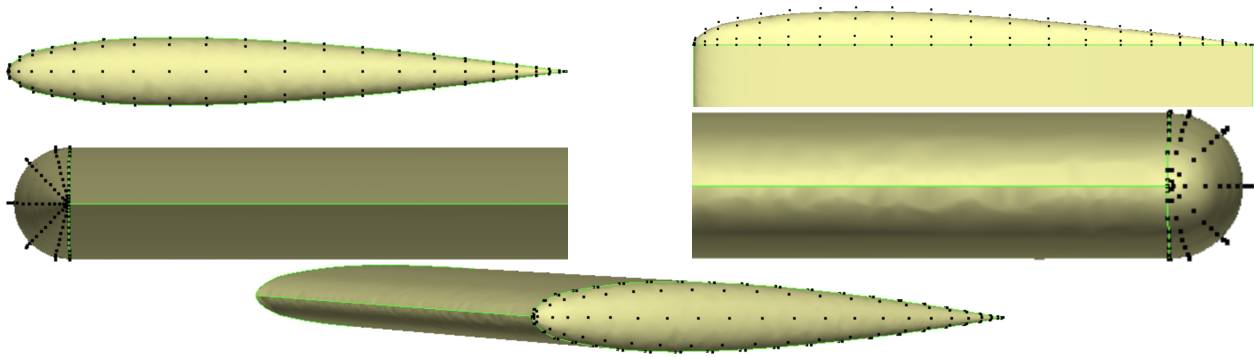
Fig. 11   The B-Spline surface and control point net defining the wingtip of a NACA 0012 airfoil.

In the u-direction (lengthwise along the airfoil) of the B-Spline surface there are 25 control points and in the v-direction (bottom to top) there are 7 control points. In total, there are 175 control points defining the B-Spline surface in Fig. 11. The first and last control points in both the u and v directions are kept constant to avoid any opening up of the wingtip from the rest of the wing. Also, to avoid any changes in tangency, the second and second to last control points in the u and v-directions are kept constant. This leaves 63 control points, 21 in the u-direction and 3 in the v-direction, depicted in Fig. 12, as the design variables for the optimization.
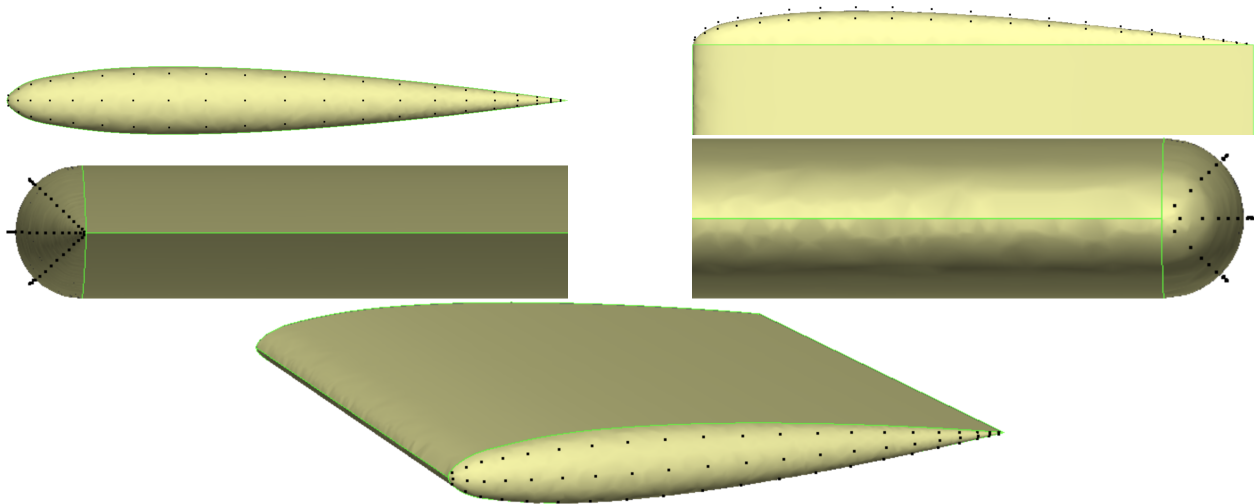
Fig. 12   The B-Spline surface with only the 63 control points used as design variables in the optimization. This is the baseline shape used as the minimum bound for the design variables and also used to compute the normal direction of the offset locations for each design variable.

Each design variable can be moved by an offset in the normal direction of the baseline wingtip shape shown in Fig. 12. This reduces the number of design parameters compared to the alternative of moving the control point locations by x, y and z offsets. The design variables were constrained to only move outward from the baseline wingtip shape. An offset value of 0.0, which corresponds to the control point coordinate in the baseline shape, is the minimum constraint for each control point. Figure 13 shows examples of three control points and their sensitivity information when each is moved independently by an offset of 0.25 from the original position of the control point in Fig. 12. All of the sensitivity calculations were verified with finite differencing. The red areas in Fig. 13 represent positive gradients, while the blue represents 0.0 gradients.

(a) Sensitivity of control point 033 pulled out by a value of 0.25.

(b) Sensitivity of control point 034 pulled out by a value of 0.25.

(c) Sensitivity of control point 035 pulled out by a value of 0.25.
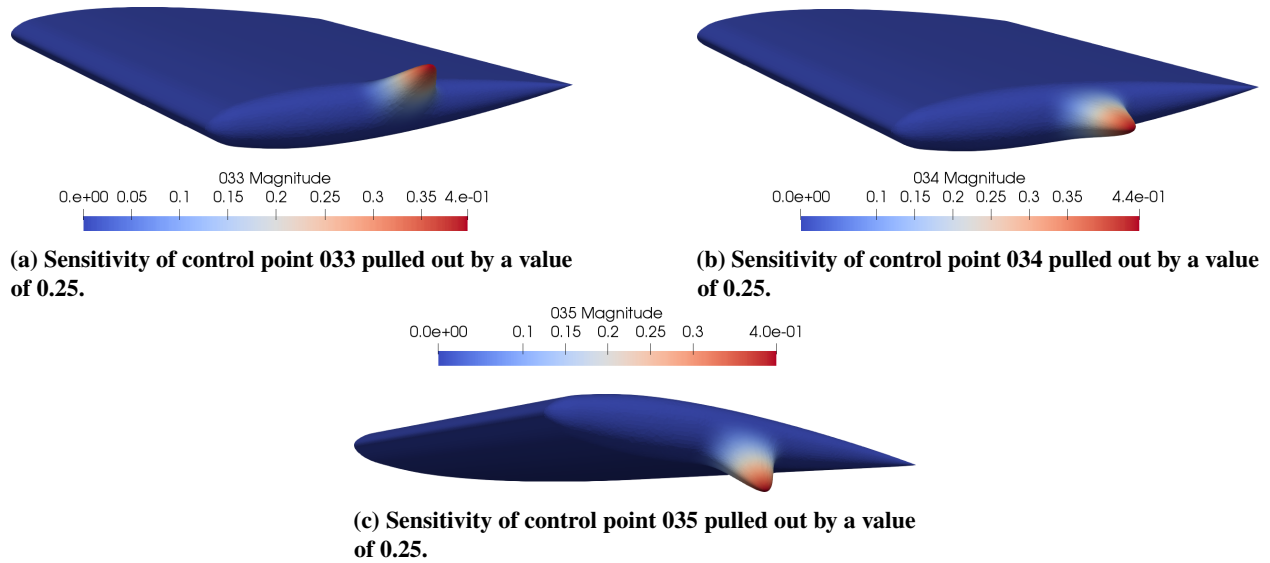
Fig. 13   Sensitivity of control point individual control points.

C. Wingtip Design with CFD Analysis

1. Shape Design with a Line Sensor

To verify the process of moving the B-Spline control points of the wingtip in 3D with `Cart3D`, a case was created to match the pressure signature to a target shape using a line sensor. The line sensor is created using `Cart3D`, and is depicted in Fig. 14 as a black line. The pressure along this line is extracted for a desired target shape. The optimization drives the shape to match the target by matching the pressure field to the extracted data. The line sensor for this case is an offset from the mean line of the airfoil and has a length of 1.3, extending slightly past the unit chord of the airfoil. The target shape is the baseline wingtip in Fig. 12, with no control points moved. This is setup such that the optimal solution is when all of the design variables have values of 0.0.
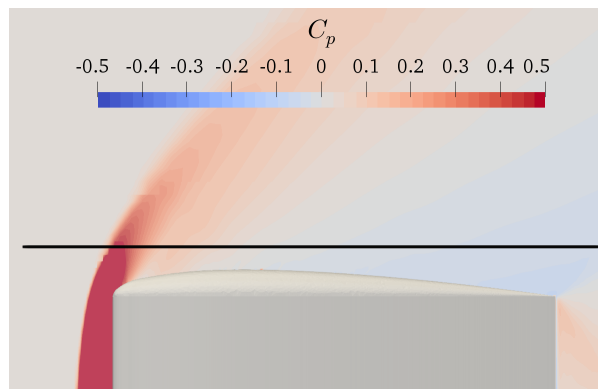
Fig. 14   Target geometry of the line sensor (represented by the black line). No control points have offsets.

The initial geometry for the optimization has each of the 21 points of the middle row of the B-Spline surface in the v-direction shown in Fig. 12 pulled out by an offset of 0.05 and is depicted in Fig. 15 on the left. `Cart3D` is executed with a Mach number of 1.5, a 0 degree angle-of-attack, and no adaptation on the flow mesh. A flow mesh with 10 levels of refinement and approximately 1.25 million cells is used. The SNOPT algorithm in the `Cart3D` design framework is used for optimization. After approximately 90 design iterations, the best geometry, shown in Fig. 15 on the right, reverted to the target shape with the exception of the tail. The very last control point at the tail of the wingtip has an offset value of approximately 0.02, while the rest of the control point design variables approximated 0.0 as they

10

were in the target shape. The offset of the tail control point is likely because the influence of the tail of the wingtip is downstream from the line sensor. The pressure signature of the best geometry from the optimization and the target geometry is plotted in Fig. 16, and shows a close match between the two pressure signatures.
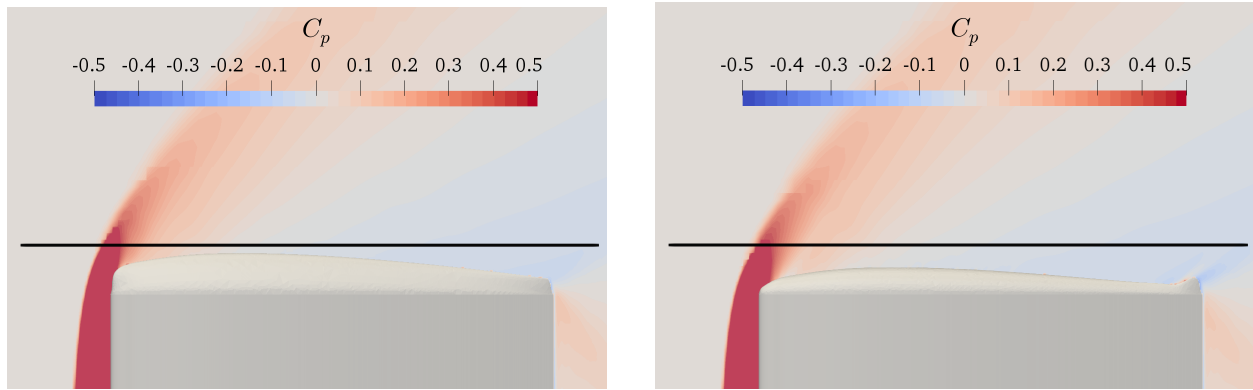
(a) Initial geometry for the line sensor optimization. All control points of the central B-Spline running along the chord of the airfoil have offset values of 0.05.

(b) Best geometry from the line sensor optimization.

Fig. 15   Pressure of the initial and best shapes from the optimization, with the line sensor in black.
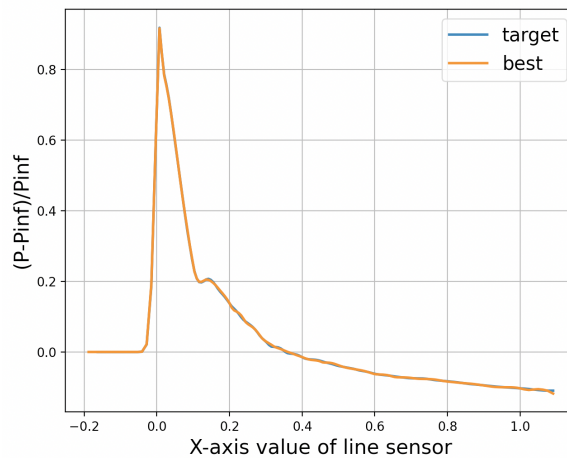
Fig. 16   Pressure signatures of the line sensor.

2. Shape Design Minimizing Drag and Maintaining Lift

After verifying the optimization process with the line sensor case, `Cart3D` is used to test shaping a wingtip with an objective function of minimizing the coefficient of drag while constraining the coefficient of lift to that of the initial wingtip geometry of the optimization. The constraint on lift is added to to prevent the optimization from driving the shape to the trivial baseline with all coefficients set to zero. The lift constraint makes it necessary for some of the area of the initial wingtip to be maintained. For the initial geometry of the optimization, the control points in the central row along the chord were given values of 0.25, with the leading edge control point values gradually increasing up to 0.25 to create a smooth leading edge. This initial geometry for the optimization is shown in Fig. 17. There is a minimum constraint of 0.0 and a maximum constraint of 0.30 for all 63 of the design parameters.

11
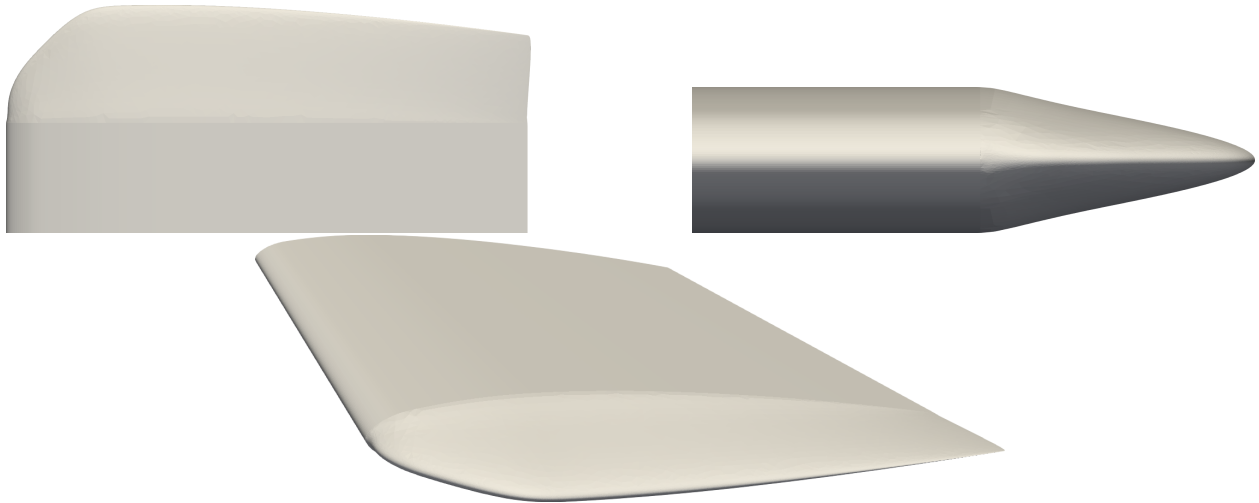
Fig. 17   Initial geometry for the optimization of the wingtip at Mach= 1.5 for the cases of $\alpha = 2, 8$ and 16.

This geometry was analyzed with `Cart3D` at a Mach number of 1.5 for angle-of-attacks of 2, 8, and 16 degrees. The minimum constraint for each angle-of-attack case was the coefficient of lift of the initial geometry in Fig. 17 at the respective angle-of-attack, hence, the lift at the full extension of the shape could not decrease as drag is minimized. As in the line sensor case, a fixed grid with no adaptive cycles and the SNOPT algorithm is used in the optimization. The grid used in the optimization has 10 levels of refinement and approximately 1.25 million cells.

For the best shape from the optimization of the $\alpha = 2°$ case, the leading half of the wingtip is pushed up against the minimum bound of 0.0, while the design variables in the trailing half maintained close to their initial values of 0.25. The best shape result from the optimization is shown in Fig. 18. The minimum coefficient of lift of 0.10 for this angle-of-attack is maintained in the best geometry, and the drag is reduced from approximately 0.110 to 0.103. The optimization completed after about 80 design iterations. The control points in the row above and the row below the center row kept their initial values of 0.0 in the best shape. The pressure profiles of the initial and best shapes for the $\alpha = 2°$ are shown in Fig. 19.
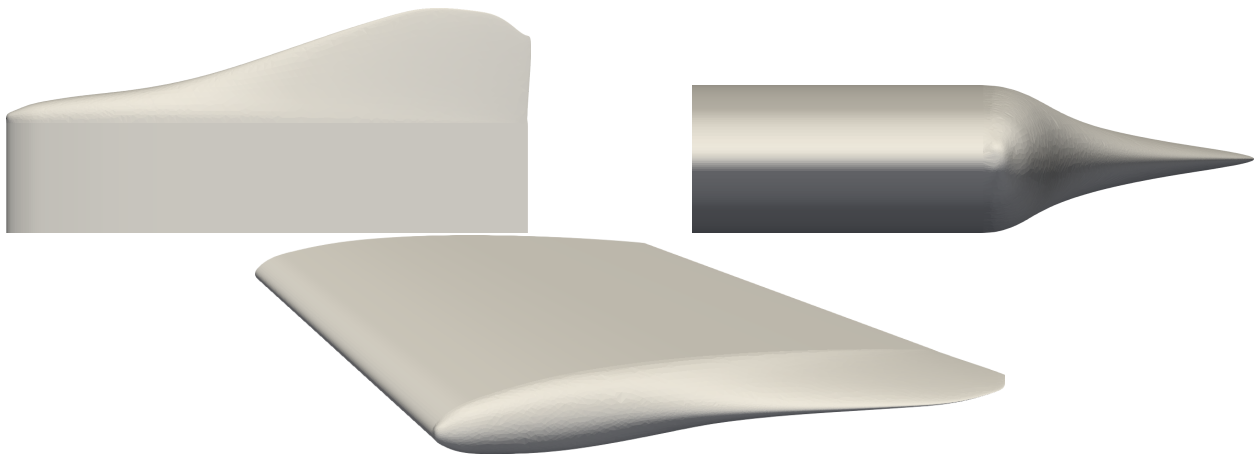
Fig. 18   Best geometry of the optimization for the $\alpha = 2°$ case.
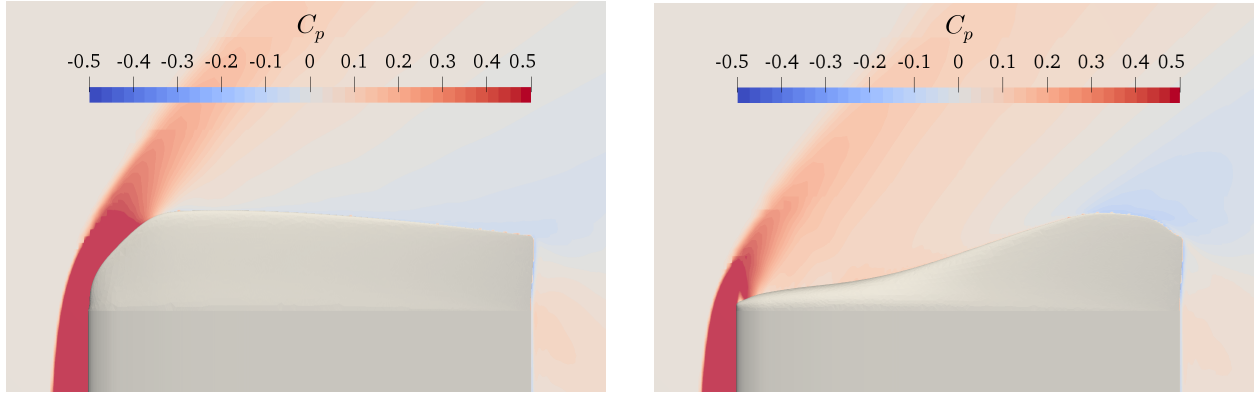
Fig. 19 Initial and best geometry pressures for the $\alpha = 2°$ case. The constraint on C_L is 0.10.

For the case with $\alpha = 8°$, the trailing half of the wingtip maintains close to the initial values of 0.25 for the design variables. At this angle-of-attack, the coefficient of lift is approximately 0.41 for the initial geometry, and this value is used as the minimum for the lift constraint. The coefficient of drag is approximately 1.65 in the initial wingtip shape and 1.57 in the best wingtip shape. The pressure profiles of the initial and best shapes for the $\alpha = 8°$ are shown in Fig. 21.
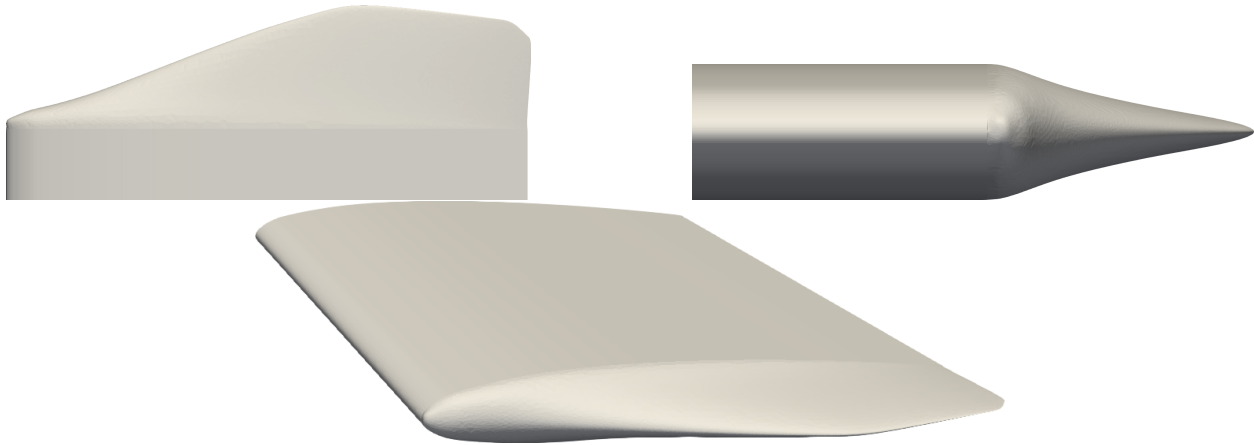
Fig. 20 Best geometry of the optimization for the $\alpha = 8°$ case.
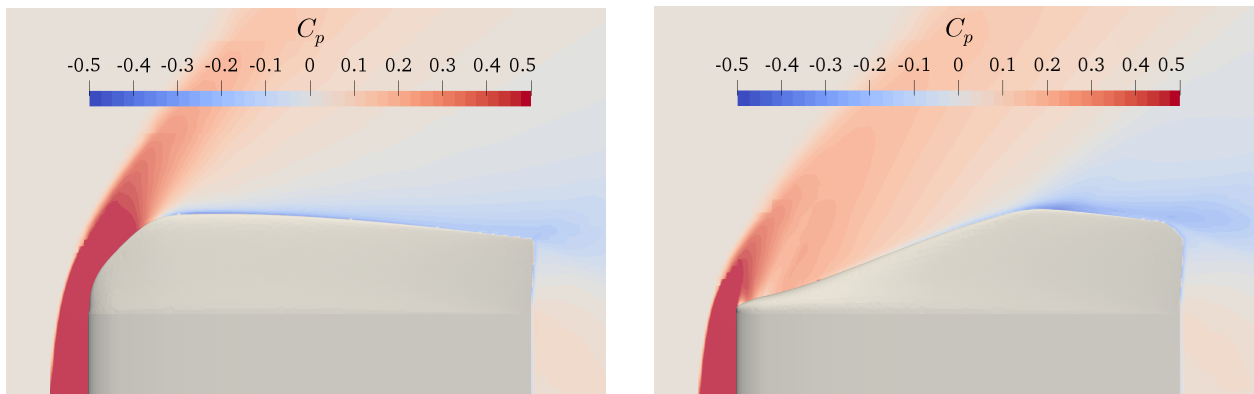
Fig. 21 Initial and best geometry pressures for the $\alpha = 8°$ case. The constraint on C_L is 0.41.

Lastly, for the case with $\alpha = 16°$, more of the design variables toward the leading edge of the wingtip have values close to the initial values of 0.25, with two of the control points around the midway point bumping up against the 0.30

maximum constraint. Like in the other angle-of-attack cases, the control points not in the middle row remained at 0.0 in the best shape of the optimization. The minimum constraint on the coefficient of lift is 0.81 for this angle-of-attack, and the coefficient of drag is approximately 0.33 in the initial wingtip shape and 0.32 in the best wingtip shape from the optimization. The pressure profiles of the initial and best shapes for the $\alpha = 16°$ are shown in Fig. 23.
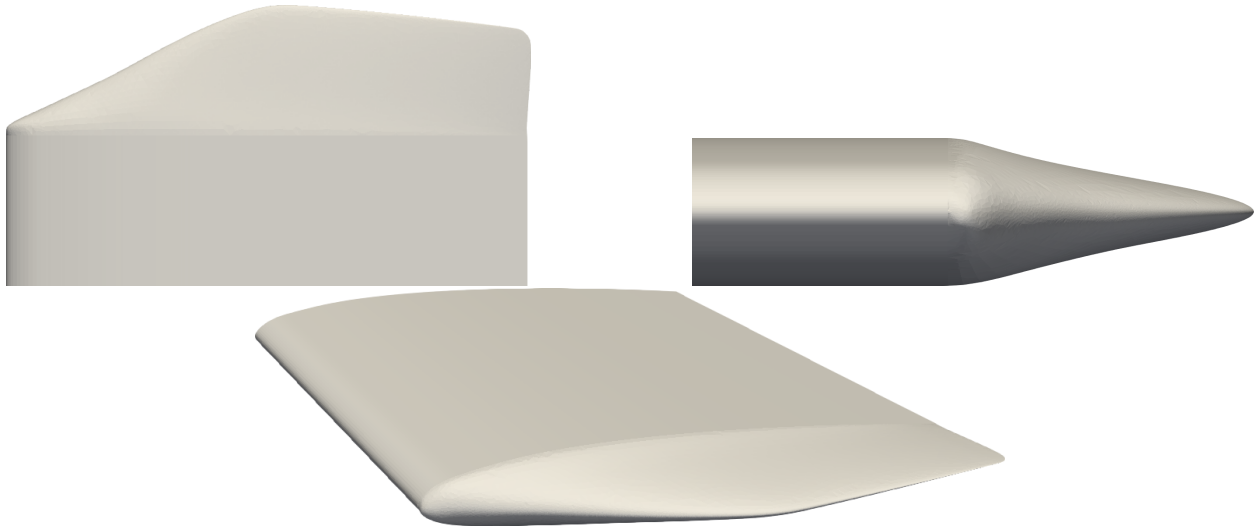
Fig. 22   Best geometry of the optimization for the $\alpha = 16°$ case.
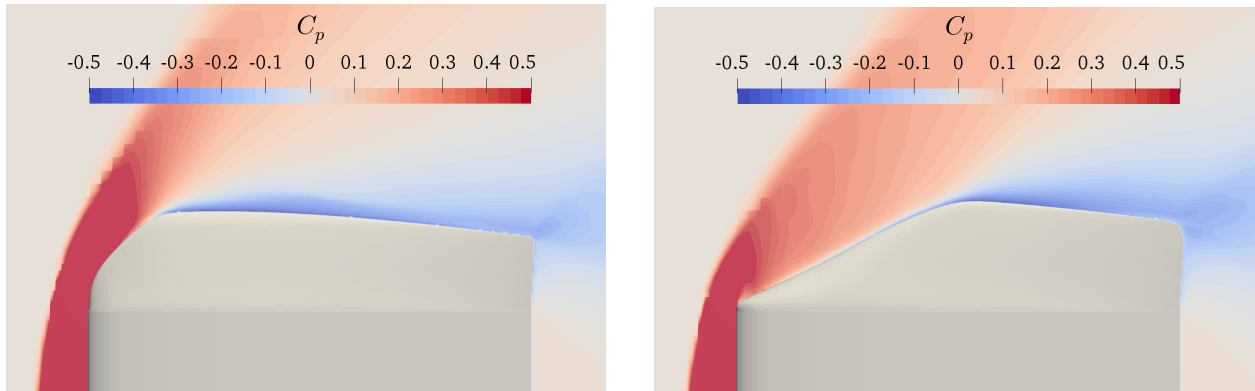
Fig. 23   Initial and best geometry pressures for the $\alpha = 16°$ case. The constraint on C_L is 0.81.

The coefficient of drag and lift values are plotted for each of the optimization in Fig. 24. The objective function, which is minimizing the coefficient of drag, is seen to converge in all three optimizations. Additionally, the minimum constraint on the coefficient of lift for each case is satisfied in the best geometry shapes.
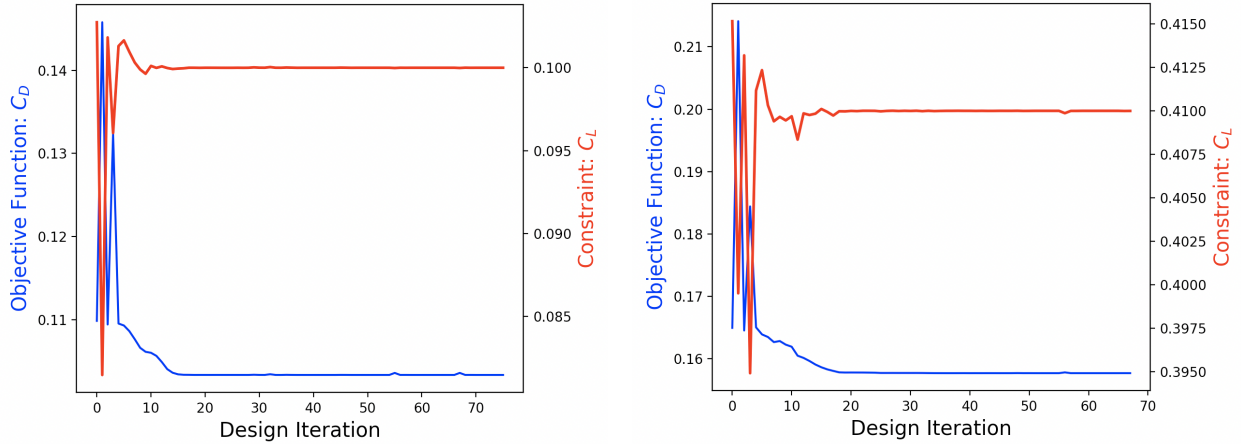
(a) Alpha = 2 degrees. Coefficient of Lift minimum of 0.10.

(b) Alpha = 8 degrees. Coefficient of Lift minimum of 0.41.
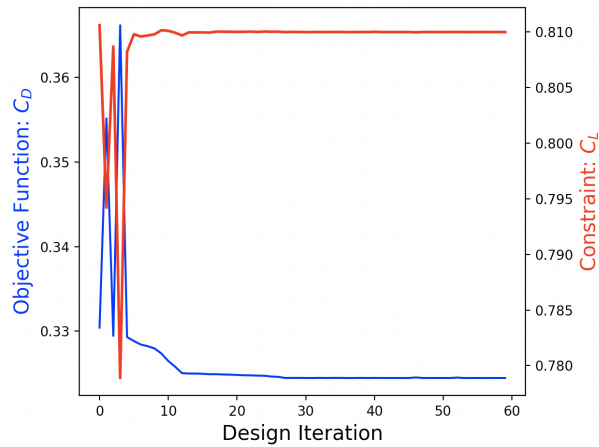
(c) Alpha = 16 degrees. Coefficient of Lift minimum of 0.80.

Fig. 24   Objective function and constraint graphs for minimizing drag and holding lift.

IV. Conclusions

A method for aerodynamic design which can combine traditional CAD-like parametric solid model construction with freeform-like local deformation (using B-splines) driven by optimization can provide an effective design strategy. The notion is to use parametric design where the traditional aerodynamic parameters are in play in order to reach an analysis driven optimal shape for this first phase. But at this point there may be places in the design that need additional work (for example wingtips, nacelle shapes, struts, the wing-fuselage junction and others) where the parameterization does not allow for the malleability of shape needed. The underlying surfaces, if not already B-Splines can be converted. A subset of the control points of these regions can now be adjusted by the analysis driven optimization in order to *sculpt* these regions while leaving the rest of the shape *frozen*.

The freeform method described in this paper uses the geometry generation software within ESP and, as presented here, the CFD analysis and adjoint design framework in `Cart3D`. This part of the design strategy is demonstrated in 2D and 3D on airfoil and wingtip geometries where it is shown that the control point locations can be effectively used as parameters which are moved by the design framework to find optimal shapes satisfying an objective function and constraint(s).

Acknowledgements

References

[1] Pironneau, O., "On optimum design in fluid mechanics," *Journal of fluid mechanics*, Vol. 64, 1974, pp. 97–110.

[2] Kim, J.-E., and Rao, V. N., and Koomullil, R. P., and Ross, D. H., and Soni, B. K., and Shih, A. M., "Development of an efficient aerodynamic shape optimization framework," *Mathematics and Computers in Simulation*, Vol. 79, No. 8, 2009, pp. 2373–2384.

[3] Nadarajah, S. K. and Tatossian, C, "Multi-objective aerodynamic shape optimization for unsteady viscous flows," *Optimization and Engineering*, Vol. 11, No. 1, 2010, pp. 67–106.

[4] D. J. Poole, and C. B. Allen, and T. C. S. Rendall, "Application of Control Point-Based Aerodynamic Shape Optimization to Two-Dimensional Drag Minimization," AIAA 2014-0413, January 2014.

[5] Antony Jameson, and Sriram Shankaran, and Luigi Martinelli, "Continuous Adjoint Method for Unstructured Grids," AIAA 2008-1226, May 2008.

[6] Marian Nemec and Michael J. Aftosmis, "Parallel Adjoint Framework for Aerodynamic Shape Optimization of Component-Based Geometry," AIAA 2011-1249, January 2011.

[7] Fudge, D., and Zingg, D. W., and Haimes, R., "A CAD-Free and a CAD-Based Geometry Control System for Aerodynamic Shape Optimization," AIAA 2005-0451, January 2005.

[8] Hugo Gagnon and David W. Zingg, "Two-Level Free-Form Deformation for High-Fidelity Aerodynamic Shape Optimization," AIAA 2012-5447, September 2012.

[9] George R. Anderson, and Michael J. Aftosmis, and Marian Nemec, "Parametric Deformation of Discrete Geometry for Aerodynamic Shape Design," AIAA 2012-0965, January 2012.

[10] Nemec, M., and Aftosmis, M. J., and Pulliam, T. H., "CAD-Based Aerodynamic Design of Complex Configurations Using a Cartesian Method," AIAA 2004-0113, January 2004.

[11] de Boor, C., *A Practical Guide to Splines,*, Springer-Verlag, 1978.

[12] Amoiralis, E. I. and Nikolos, I. K., "Freeform Deformation Versus B-Spline Representation in Inverse Airfoil Design," *Journal of Computing and Information Science in Engineering*, Vol. 8, No. 2, 2008, pp. 152–172.

[13] Haimes, R., and Dannenhoffer, J, "The Engineering Sketch Pad: A solid-modeling, feature-based, web-enabled system for building parametric geometry," 2013.

[14] Xu, Shenren and Timme, Sebastian and Mykhaskiv, Orest and Müller, Jens-Dominik, "Wing-body junction optimisation with CAD-based parametrisation including a moving intersection," *Aerospace Science and Technology*, Vol. 68, 2017.

[15] Marshall C. Galbraith and Steven R. Allmaras and David L. Darmofal, "A verification driven process for rapid development of CFD software," AIAA 2015-0818, January 2015.

[16] Piegl, Les and Tiller, Wayne, *The NURBS Book*, 2nd ed., Springer-Verlag, New York, 1997.

[17] Charles L. Ladson, and Cuyler W. Brooks, Jr., and Acquilla S. Hill, and Darrell W. Sproles, "Computer Program to Obtain Ordinates for NACA Airfoils," *National Aeronautics and Space Administation*, 1996.

[18] Johnson, S. G., "The NLopt nonlinear-optimization package," 2007.

[19] J. Nocedal, "Updating quasi-Newton matrices with limited storage," *Math. Comput.*, Vol. 35, 1980, pp. 773–782.

[20] D. C. Liu and J. Nocedal, "On the limited memory BFGS method for large scale optimization," *Math. Programming*, Vol. 45, 1989, pp. 503–528.

[21] Powell, M. J. D., "A direct search optimization method that models the objective and constraint functions by linear interpolation," *Advances in Optimization and Numerical Analysis*, 1994, pp. 51–67.

[22] Marian Nemec and Michael J. Aftosmis, "Parallel Adjoint Framework for Aerodynamic Shape Optimization of Component-Based Geometry," *AIAA*, Vol. 49, January 2011.

[23] Dannenhoffer, J. F., and Haimes, R., "Using Design-Parameter Sensitivities in Adjoint-Based Design Environments," *AIAA Paper 2017–0139*, June 2017.

[24] P. E. Gill, Michael W. Murray, and A. Saunders, "SNOPT: An SQP algorithm for large-scale constrained optimization," *SIAM Journal on Optimization*, Vol. 12, 1997, pp. 979, 1006.

[25] George R. Anderson, and Marian Nemec, and Michael J. Aftosmis, "Aerodynamic Shape Optimization Benchmarks with Error Control and Automatic Parameterization," AIAA 2015-1719, June 2015.

[26] Haimes, R., and Dannenhoffer, J, "On The Construction of Aircraft Conceptual Geometry for High-Fidelity Analysis and Design," 2012.

[27] Galbraith, M. C., and Haimes, R., "A Parametric G1-continuous Rounded Wing Tip Treatment for Preliminary Aircraft Design," *AIAA Paper 2022*, January 2022.